Article:
Potter, DG orcid.org/0000-0002-0656-5657, Blitz, MA orcid.org/0000-0001-6710-4021 and Seakins, PW (2019) A generic method for determining R + O_2 rate parameters via OH regeneration. Chemical Physics Letters, 730. pp. 213-219. ISSN 0009-2614

https://doi.org/10.1016/j.cplett.2019.06.014

A Generic Method for Determining R + O_2 Rate Parameters via OH Regeneration

David G. Potter[1,2], Mark A. Blitz*[1,3] and Paul W. Seakins*[1,3]

[1]School of Chemistry, University of Leeds, Leeds, LS2 9JT, UK

[2]School of Chemical and Process Engineering, University of Leeds, Leeds, LS2 9JT, UK

[3]National Centre for Atmospheric Science, University of Leeds, Leeds, LS2 9JT, UK

Abstract

Reactions of fuel derived radicals, R, and oxygen, are of interest for low temperature combustion and autoignition. A method for measuring R + O_2 rate coefficients based on the real time regeneration of OH radicals following initiation of the reaction via OH + RH is presented; values for k_{R+O2} can be extracted from the resulting biexponential OH profiles. The rate coefficient for the reaction of CH_3OCH_2, with O_2, at 291 – 483 K, in 4.1 – 32.6 Torr of nitrogen are reported. At room temperature, $k_{CH3OCH2+O2} = (0.94 \pm 0.04) \times 10^{-11}$ cm^3 molecule^{-1} s^{-1}, where the error represents statistical uncertainty at the 2σ level.

1. Introduction

Fuel derived radicals, R, produced by abstraction of a hydrogen (R1) by a radical species, X (X = OH, O, H, HO_2 etc), are an integral species in low temperature combustion chemistry. In a typical low temperature oxidation mechanism, the reaction of R with molecular oxygen leads to formation of the RO_2 radical (R2), which can undergo internal rearrangement to form the QOOH radical (R3) where the radical centre is now located on a carbon atom. Decomposition of this QOOH radical (R4) in a chain-propagating reaction, is in competition with a second oxygen addition, to form a QOOH-peroxy species (R5). Under the appropriate conditions, this O_2QOOH species can react to ultimately produce multiple radicals (R6). This chain-branching step is believed to be key to the autoignition of fuels [1-3].

$$X + RH \rightarrow HX + R \quad \text{(R1)}$$

$$R + O_2 \leftrightarrow RO_2 \quad \text{(R2)}$$

$$RO_2 \leftrightarrow QOOH \quad \text{(R3)}$$

$$QOOH \rightarrow OH + \text{carbonyl} \quad \text{(R4)}$$

$$QOOH + O_2 \rightarrow O_2QOOH \quad \text{(R5)}$$

$$O_2QOOH \rightarrow OH + Q'OOH \rightarrow \text{chain branching} \quad \text{(R6)}$$

Understanding the details of this mechanism is important in determining the autoignition properties of a fuel. The recent development of Homogeneous Charge Compression Ignition (HCCI) and related engines, whose operation depends on autoignition, provides added impetus for unravelling the chemical details of these mechanisms for both fossil fuels and biofuels [4,5].

The methoxy methyl radical (CH_3OCH_2), is the R radical formed in the low temperature oxidation system for dimethyl ether (DME, CH_3OCH_3) (R7), a potential biofuel [6,7]. The integral role R + O_2 chemistry plays in DME low temperature oxidation is evidenced by the various fates of its product (Figure 1). Oxygen addition in R8 leads to a chemically activated RO_2* peroxy radical, which can undergo pressure-dependent stabilisation to the relatively stable RO_2 radical (R9). Alternatively, the RO_2* radical has two other competing pathways. These are re-dissociation to reactants (competitive at high temperatures), or formation of QOOH* (via an internal hydrogen abstraction) followed rapidly by decomposition to OH and formaldehyde (R10), a process referred to as 'well-skipping'. Stabilisation of QOOH* is not considered, as the QOOH energy well is significantly higher than that of RO_2, thus the equilibrium of R10's initial step is shifted towards the RO_2* species.

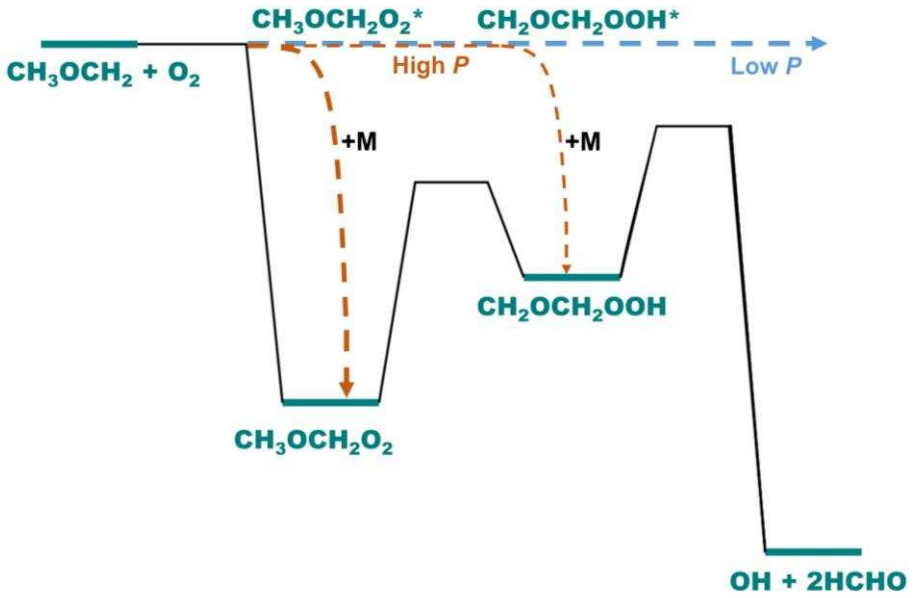

Fig. 1. Potential energy surface showing the competition between RO_2* stabilisation into RO_2/QOOH wells at high pressures (orange thick/thin line), and formation of OH at low pressures (blue line).

$$CH_3OCH_3 + OH \rightarrow CH_3OCH_2 + H_2O \quad \text{(R7)}$$

$$CH_3OCH_2 + O_2 \leftrightarrow CH_3OCH_2O_2^* \quad \text{(R8)}$$

$$CH_3OCH_2O_2^* \xrightarrow{M} CH_3OCH_2O_2 \quad \text{(R9)}$$

$$CH_3OCH_2O_2^* \leftrightarrow CH_2OCH_2OOH^* \rightarrow 2CH_2O + OH \quad \text{(R10)}$$

Previously, in order to measure the rate coefficient for R8 (k_8), a brominated molecule of DME, CH_3OCH_2Br, was used [8]. Equivalent analogues are not available for other potentially important fuels such as diethyl ether (DEE) [9]. Eskola et al. [8,10] studied the kinetics of R8 using this method, and laser flash photolysis – laser-induced fluorescence (LFP–LIF), obtaining k_8 and OH yields in nitrogen and helium, by an absolute and relative method. Generation of the R radical by Cl + DME was also used, but subsequent reactions of $(COCl)_2$ photolysis products can interfere with measurements. More importantly, the absolute determinations of the OH yield using Cl + DME or OH + DME previously conducted in this laboratory offer no information on the R + O_2 rate coefficient.

Other studies on CH_3OCH_2 + O_2 rate parameters have been carried out by Sehested et al. [11] (FTIR smog chamber), Maricq et al. [12] (transient infrared and UV), Masaki et al. [13] (laser photolysis – mass spectrometry), and Rosado-Reyes et al. [14] (transient infrared), yielding a combination of branching ratios, product yields, and rate coefficients. Studies on other R + O_2 reactions have been conducted previously, such as CH_3 + O_2 by Pilling and Smith [15] using flash photolysis and absorption spectroscopy, and several R + O_2 reactions via photoionization mass spectrometry (PIMS), [16-18] and a correlation between k_{R+O2} and the ionisation potential of the R radical has been demonstrated [19].

Here, a method for measuring both R + O_2 rate coefficients and OH yields using an OH precursor is presented. This is universal for all fuels, provided they possess the ability to well-skip sufficiently at low pressures; previous studies show this technique should be applicable for systems such as OH + ketones, [20] aldehydes, [20-26] dialdehydes, [27,28] and esters [29]. The data are validated by comparison with the previous method employed in the work of Eskola et al. [10]

2. Experimental Section

The current experimental setup has been described previously[30]. Conventional slow flow laser flash photolysis was combined with laser-induced fluorescence to monitor OH [10,24,30-32]. The reactants (DME, Argo International Ltd, 99.8%), OH precursor (generally hydrogen peroxide, H_2O_2, Sigma-Aldrich, 50% (w/w) in H_2O), buffer gas (N_2) (BOC, oxygen-free), and

O_2 (BOC, 99.5%) were flowed through calibrated mass flow controllers (MFCs) into a mixing manifold, and into the stainless steel reaction cell. Experiments were carried out at a flow rate of approximately 270 – 1100 SCCM and between 4.1 – 32.6 Torr of pressure. For experiments carried out above room temperature, the reaction cell was heated using cartridge heaters. A calibrated K-type thermocouple was used to measure the temperature close to the entrance of the cell. A capacitance manometer (MKS Baratron, 0 – 1000 Torr) was used to measure the pressure inside the reaction cell, controlled by throttling the rotary pump with a needle valve.

Contact of hydrogen peroxide with the metal pipes and consequent decomposition results in some oxygen always being delivered to the system, which was estimated to be approximately (0.6 – 2.9) × 10^{14} molecule cm^{-3} (the method for estimating this oxygen concentration is discussed in the data analysis section), and varies depending on pressure and flow.

Photolysis of the hydrogen peroxide at 248 nm was used to generate the hydroxyl radicals (R11), and was the source of OH for the majority of experiments in this work. Urea hydrogen peroxide ($CO(NH_2)_2.H_2O_2$, Sigma-Aldrich, 97%) was also used as a known OH precursor [33,34] for comparison, and CH_3OCH_2Br (Sigma-Aldrich, 90%) employed to measure R + O_2 rate coefficients using the same method as Eskola et al. [10]).

$$H_2O_2 + h\nu\ (\lambda = 248\ nm) \rightarrow 2OH \qquad (R11)$$

The OH precursor was photolysed using an excimer laser operating at 248 nm (KrF, Lambda Physik LPX 200, 10 Hz pulse repetition frequency, typical energy 40 – 80 mJ $pulse^{-1}$ cm^{-2}, beam dimensions 25 mm × 10 mm) for photolysis. The photon density was approximately 7.5 × 10^{16} photons cm^{-2}, and the typical initial OH concentration, $[OH]_0$, was ~1 × 10^{12} molecule cm^{-3}. On-resonance laser-induced fluorescence was used, probing the OH radicals at ~308 nm, corresponding to the OH $Q_1(2)$ rotational line of the $A^2\Sigma(v' = 0) \leftarrow X^2\Pi(v'' = 0)$ transition. The probe laser light was obtained from the output of an Nd:YAG-pumped (Continuum Precision II, 532 nm) dye laser (Sirah PRSC-DA-24, 10 Hz, energy <0.1 mJ $pulse^{-1}$, 3 mm beam diameter, DCM Special dye). The dye laser output at ~616 nm was doubled to output ~308 nm. Fluorescence from the OH radicals at ~308 nm was detected by a photomultiplier (Electron Tubes), after passing through a filter ((308 ± 5) nm, Barr Associates). A digital oscilloscope (LeCroy LT 372) integrated the fluorescence signal, before transferring the output to the personal computer for collection and analysis, where the fluorescence signal was normalised for probe laser power.

To build up a time-dependent trace of OH fluorescence signal, the time delay between the photolysis and probe lasers was varied using a delay generator, with a typical decay trace consisting 230 points, each averaged 10 – 30 times. The total gas flow ensured each laser shot photolysed a fresh sample of gas. Probing on–resonance necessitated using a delay (~30 ns) before analysing the fluorescence to avoid detecting the scatter pulse from the probe laser. A typical OH decay for the reaction of OH with DME, with some OH regeneration, is shown in the inset to Figure 2.

3. Chemical Activation Data Analysis

Decays showing chemical activation in the presence of low oxygen ($[O_2] \approx (0.7 – 26) \times 10^{14}$ molecule cm^{-3}) require complex analysis. Regeneration of OH results in biexponential kinetic decays, where the initial fast decay is the reaction between OH and DME, and the tail portion of the decay contains information about the OH formation. An equation derived from Scheme 1 was used to analyse these traces.

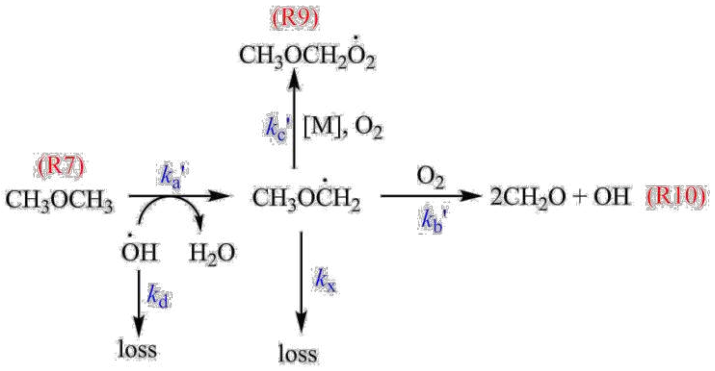

Scheme 1. Reaction scheme for analysis of OH regeneration traces. This scheme represents the route following initial H abstraction from DME. Parameters used in the biexponential equation are in blue.

Here, the only routes considered for the fate of the R radical are reaction with O_2 followed by stabilisation to RO_2 (R9), reaction with O_2 followed by formation of OH (chemical activation, R10), and another minor loss process for the R radical, potentially self-reaction. The total rate coefficient for R + O_2 is the sum of the rate coefficients from R9 and R10 ($k'_8 = k'_b + k'_c$). The following equations (E1 – E5) were used to fit the traces:

$$OH = OH_0 \times \left[\left(\frac{-(k_d+k_a') - \lambda_2}{\lambda_1 - \lambda_2}\right) \times \left(e^{\lambda_1 \times t} - e^{\lambda_2 \times t}\right) + e^{\lambda_2 \times t}\right] \quad \text{(E1)}$$

$$\lambda_1 = \frac{\left(-M1 + \sqrt{M1^2 - 4M2}\right)}{2} \quad \text{(E2)}$$

$$\lambda_2 = \frac{\left(-M1 - \sqrt{M1^2 - 4M2}\right)}{2} \quad \text{(E3)}$$

$$M1 = k_d + k_a' + k_b' + k_c' \quad \text{(E4)}$$

$$M2 = (k_d + k_a') \times (k_b' + k_c') - (k_a' k_b') \quad \text{(E5)}$$

Here, k_a' = pseudo-first order rate coefficient for R7, k_d = rate coefficient for OH loss in the absence of DME (fixed to the value measured when only OH precursor is present), and the terms λ_1 and λ_2 are expanded fully in E2 – E5. The terms k_b' (pseudo-first order rate coefficient for OH regeneration from R + O_2) and k_c' (pseudo-first order rate coefficient for R radical reacting with O_2 and not producing OH) are both present in λ_1 and λ_2. Reactions were studied under pseudo-first order conditions where [DME] >> [OH]. [OH] is therefore proportional to the fluorescence intensity, and thus the exact concentration of OH does not need to be known.

For robust parameter retrieval, global fitting was used to analyse several kinetic traces as a function of [DME] at once ($k_a' = k_7$[DME] for each trace), and share the bimolecular rate coefficient for OH + DME (k_7) and R + O_2 (k_8) between decays. Similarly, the k_b' and k_c' parameters have been related to their bimolecular rate coefficient counterparts to globally share these parameters across all traces. Additionally, O_2x (unavoidable O_2 arising from H_2O_2 decomposition) has been accounted for, and k_x was introduced as a small loss of the R radical to achieve good fits at the very lowest [O_2] traces, where O_2 addition was in competition with other possible processes (loss of R, R + R, R decomposition). For single trace analysis using E1, k_x is not present, or even obtainable, but this does not affect the measured value for k_8, as the straight line in Figure 2 would simply be shifted down if k_x was accounted for (k_x is constant across a range of [O_2]). The intercepts, and therefore [O_2x] will be slightly affected by the exclusion of k_x for single trace analysis, but these are compared to those from global analysis in the SI (Figure S1). Ultimately multiple traces are required to yield information about k_x. All parameters are listed below in Table 1.

Table 1

Description of parameters used in the global analysis treatment of data. Details on whether these parameters are fixed (input), and shared (across multiple traces where pressure and temperature is constant) or local are included. The full Origin C code is included in the SI.

Parameter		Definition	Relationship	Share	Fix
k_a'		Pseudo-first order rate coefficient for OH + DME	$= k_7[DME]$	No	No
	k_7	OH + DME bimolecular rate coefficient		Yes	No
	[DME]	DME concentration		No	Yes
k_b'		Pseudo-first order rate coefficient for OH formation	$= k_b([O_2]+[O_2x])$	No	No
	k_b	$R + O_2 \rightarrow OH$ bimolecular rate coefficient		Yes	No
	$[O_2]$	Oxygen concentration added		No	Yes
	$[O_2x]$	Oxygen concentration always present in system		Yes	No
k_c'		Pseudo-first order rate coefficient for $R + O_2$ not yielding OH	$= k_c([O_2]+[O_2x]) + k_x$	No	No
	k_c	$R + O_2 \rightarrow RO_2$ bimolecular rate coefficient		Yes	No
	k_x	First order rate coefficient for loss of R radical		Yes	No
OH yield		Yield of OH formed from $R + O_2$	$= k_b/k_8$	Yes	No
	k_8	$R + O_2$ bimolecular rate coefficient	$= \frac{(k_b'+k_c'-k_x)}{([O_2]+[O_2x])}$	Yes	No
OH_0		Initial signal intensity		No	No
k_d		First order rate coefficient for loss of OH		Yes	Yes

Data analysis using E1 allows the total rate coefficient for R8 (k_8) to be measured using a pseudo-first order bimolecular treatment of the total removal of the RO_2 radical ($k_b' + k_c'$) as a function of $[O_2]$. After the initial abstraction (R7) occurs, the CH_3OCH_2 radical concentration can be no higher than $[OH]_0 \approx 10^{12}$ molecule cm^{-3}, thus the addition of $[O_2] \approx (0.7 – 26) \times 10^{14}$ molecule cm^{-3} allows k_{R+O2} to be measured under pseudo-first order conditions, where $R + O_2$ is the rate determining step. Figure 2 shows an example biexponential decay (inset), and a bimolecular plot determining k_8.

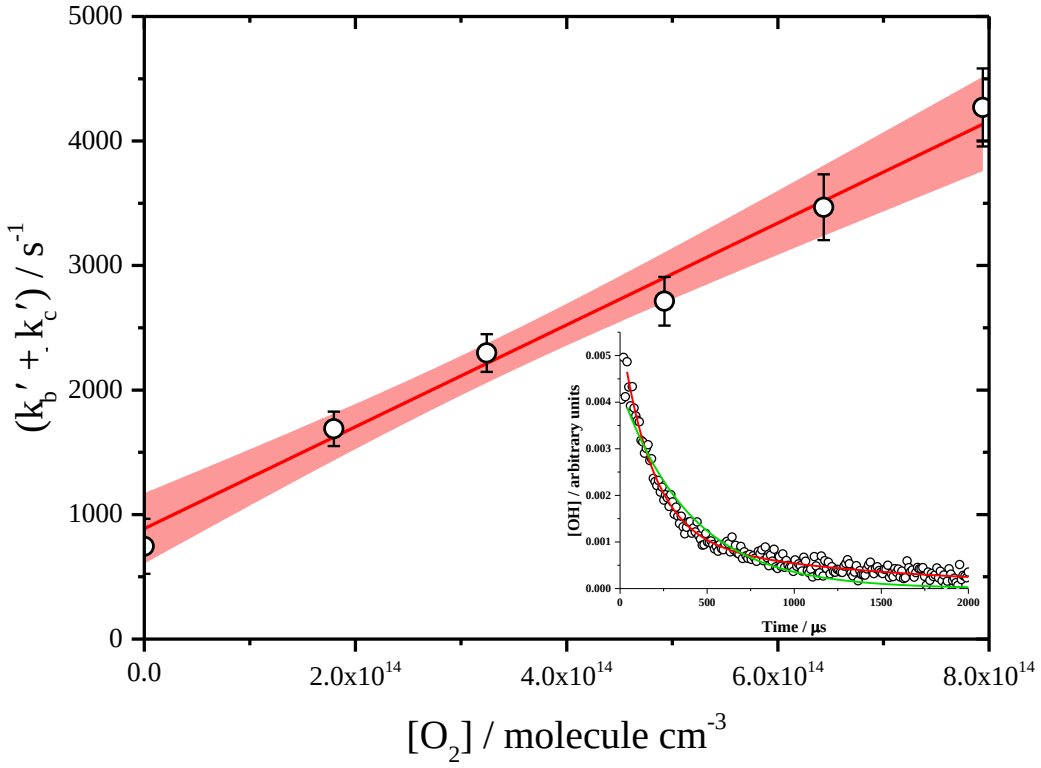

Fig. 2. Bimolecular plot for the determination of the R + O_2 rate coefficient, at (483 ± 5) K, 10.8 Torr, [DME] = (0.67 – 1.01) × 10^{15} molecule cm^{-3}. k_8 = (4.09 ± 0.73) × 10^{-12} cm^3 $molecule^{-1}$ s^{-1}. The shaded area represents the bounds of the 95% confidence limits. The inset shows an example biexponential decay, where the parameters recovered were k_b' = (870 ± 190) s^{-1}, k_c' = (820 ± 200) s^{-1}, k_d = 400 s^{-1} (fixed from OH decay when [DME] = 0), and k_a' = (4170 ± 340) s^{-1}, at [O_2] = 1.8 × 10^{14} molecule cm^{-3}, and experimental conditions were the same as for the bimolecular plot. The green line compares a single exponential decay fit where k_a' = (2490 ± 150) s^{-1}. All errors represent 2σ statistical uncertainties.

The intercept for a bimolecular plot of this nature can be related to the amount of oxygen in the system by default (O_2x). E6 shows that [O_2x] = intercept/k(R+O_2).

$$(k_b'+k_c') = k(\mathrm{R+O_2})[\mathrm{O_2}] + (k(\mathrm{R+O_2})\,[\mathrm{O_2x}]) \qquad \text{(E6)}$$

Furthermore, from the biexponential analysis (using E1), the OH yield can be obtained through a relationship between k_b' and k_c' (E7), that is, the ratio between R + O_2 leading to OH, and the total removal of R by O_2 (see Scheme 1). Loss of R is also accounted for.

$$\text{OH yield \%} = \frac{k_b'}{k_b' + k_c' - k_x} \times 100 \qquad \text{(E7)}$$

For this biexponential analysis method to work as precisely as possible, the separation of the two time constants for the equation (λ_1 and λ_2 (containing the information on OH + DME and removal of R respectively)) should be pronounced, with $\lambda_1 > \lambda_2$. Experimentally, a clear separation can be achieved by keeping [DME] as high as possible (and thus k_a' fast), and [O_2] low, in order to keep the total rate of removal of the RO_2 radical ($k_b' + k_c'$) slow in comparison to k_a'. As λ_1 and λ_2 become closer together, or λ_2 becomes larger than λ_1, the OH decay becomes a less clear biexponential trace, and tends towards a single exponential decay. Additionally, under high oxygen conditions, it is possible that R + O_2 is no longer the rate-determining step. Under non-ideal conditions, analysing the data biexponentially yields poorer-defined parameters, with larger uncertainties. This is especially problematic under conditions where [O_2x] is high initially, and therefore a reduced range of [O_2] is available for determination of k_8 using a bimolecular plot. In the SI, kinetic parameters obtained using the H_2O_2/urea precursor are presented, where the background O_2 was much higher compared with the H_2O_2/H_2O precursor (Figure S2). Oxygen has been detected as a major decomposition product of urea hydrogen peroxide previously.[33] The uncertainties on k_8 measured from urea experiments were larger, and k_8 itself generally faster (Figure S3), even when the time constants did not overlap, possibly indicating R + O_2 was no longer the rate determining step in OH regeneration (once the rate of OH regeneration becomes fast compared to OH loss via reaction with DME, the decays will again become exponential). OH yields were always measured reliably (Figure S4).

The bimolecular plots (Figure 2) are weighted fits to the data, to account for the uncertainty in values of ($k_b' + k_c'$). All values reported in this work are from global analysis, including k_8; Figure 2 is purely for illustrative purposes. For values of k_8 measured using the H_2O_2/urea precursor included in the SI , k_8 was obtained using the single trace analysis method in Figure 2, and then fixed in the global determination of other parameters.

A simple chemical model generated in the numerical integrator package Kintecus[35] was used to demonstrate the poor ability to retrieve k_8 from data under less-than-ideal conditions. Here, the only parameters simulated were $k_7 = 2.93 \times 10^{-12}$ cm^3 molecule^{-1} s^{-1} (based on room temperature k_7 Arrhenius parameterisation by Carr et al. [36]), $k_8 = 1 \times 10^{-11}$ cm^3 molecule^{-1} s^{-1} and OH yield = 70%. Kintecus was used to generate traces over a range of [O_2] = (0 and $10^{13} – 10^{16}$) molecule cm^{-3}, for [DME] = 5×10^{13} molecule cm^{-3} and [DME] = 5×10^{14} molecule cm^{-3}, in order to simulate a set of data under ideal (high [DME]), and non-ideal (low [DME]) conditions. Figure S5 shows the bimolecular determinations of k_8 from both sets

of simulated experiments, where the rate coefficient returned at high [DME] was closer to the true value used for the simulated data, and the uncertainty in the low [DME] determination is much greater. Further discussion is included in the SI (Figures S6-S9).

The Kintecus model was also used to investigate possible complexities from radical-radical reactions. In our experiments, no variation in the kinetics or yields (based on single trace analysis) was observed as laser power was varied by 50% suggesting a limited role for radical-radical reactions. In the model secondary chemistry such as $CH_3OCH_2O_2$ + OH was included with rate coefficients up to 1×10^{-10} cm^3 $molecule^{-1}s^{-1}$, but no significant change was observed in the returned kinetic parameters when these reactions were included in the model.

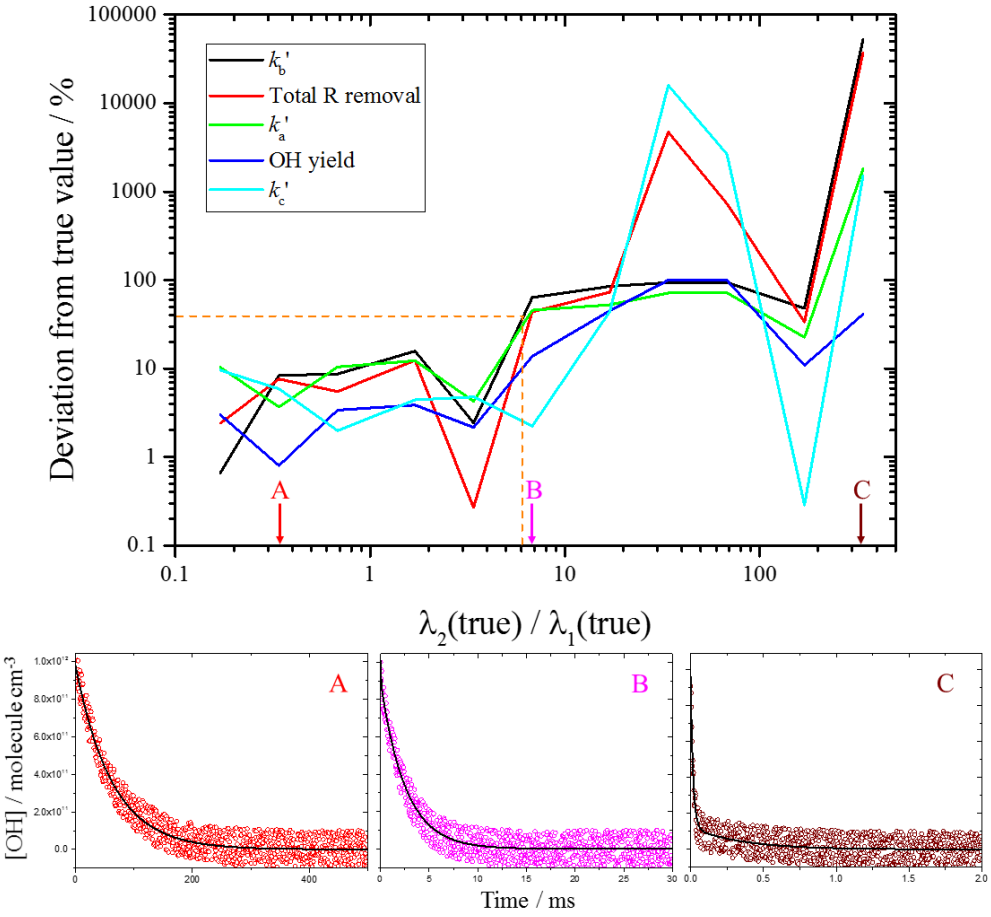

Figure 3. Deviation of returned parameters from true values as the ratio of λ_2 to λ_1 increases (% deviations here are sometimes negative, but the modulus of the values are presented). Traces generated using Kintecus (three examples shown, note the varying timescales), with ± (0 – 10)% random noise generated.

Further Kintecus simulations were used to demonstrate the deviation in returned parameters from the true values as λ_2/λ_1 increases (Figure 3). Here, the same rate parameters were simulated, but $[O_2]$ was constant at 10^{15} molecule cm^{-3}, while a range of [DME] ((1 – 2000) × 10^{13} molecule cm^{-3}) was used, to alter the degree of biexponential behaviour the traces exhibited. To achieve a deviation in the removal of the R radical rate comparable to those observed experimentally (~30 – 50%), λ_2 needed to be approximately 10 times larger than the true value of λ_1 (dashed orange line, Figure 3), however, experimentally we see large deviations at time constant ratios much smaller than this (closer to 1:1). These data were generated with ± (0 – 10)% random signal noise. With no noise, parameter retrieval was significantly better, and an even larger value of λ_2/λ_1 was required to mimic experimental deviation from true parameters (Figure S10).

More accurate parameter recovery may be as a result of the perfect data produced in Kintecus, compared to experimental data which is subject to signal noise, other processes occurring (removal of R radical by other reactions, k_x), and $[O_2x]$ present in the system, which limits the effective range of oxygen concentrations available for a bimolecular plot. OH loss in experimental data may also complicate parameter retrieval further, particularly at the lowest pressures, where diffusion plays more of a role. The same principle is demonstrated experimentally by consideration of the percentage uncertainty of ($k_b' + k_c'$) increasing as a function of $[O_2]$ (Figures S11 and S12) in H_2O_2/urea precursor measurements.

Global fitting was used to analyse traces grouped together at the same temperature and pressure, but obtained over a range of $[O_2]$. A wide variation in DME concentration was not normally used across a group of traces, and as such, obtaining k_7 from a narrow range of [DME] results in a poorly defined bimolecular rate coefficient for OH + DME, however, Figure S13 in the SI shows measurements in this work are in agreement with k_7 measured by Carr et al.[36] in this laboratory, when uncertainties are considered. 15% is approximately the greatest deviation of this work from the Arrhenius parameterisation given by Carr et al. Regardless, the ability to ascertain k_7 has no direct effect on the outcome of k_8 and OH yield determinations. O_2x and k_x from global analysis are also in the SI (Figures S1 and S14 respectively). Comparisons between k_8 retrieval by global analysis and single trace bimolecular determination of k_8 at room temperature are included in the SI, Figure S15, and differ only slightly, likely as a result of global analysis being non-weighted.

Results and Discussion

R + O_2 kinetics. Measurements of the R + O_2 rate coefficient for DME made in this work, which are comparable to those made by Eskola et al.[10] in He, and Maricq et al.[12] in N_2, are presented in Figure 4. Additionally, k_8 at all temperatures studied here are reported in Table S1. k_8 exhibits a negative temperature dependence, which is qualitatively consistent with what would be expected from a barrierless addition reaction, and was seen in the previous work.

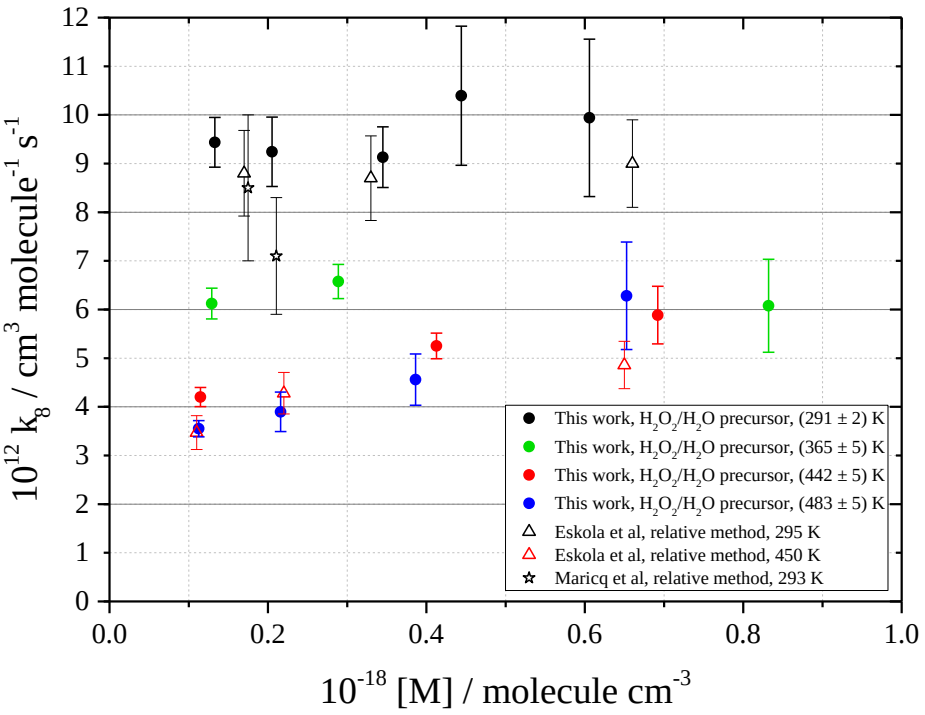

Figure 4. Comparison of R + O_2 rate coefficients measured in this work (filled symbols) with Eskola et al.[10] (open triangles) and Maricq et al.[12] (upturned triangles) as a function of pressure and temperature. For this work and Maricq et al., M = N_2, for data from Eskola et al., M = He. Error bars for this work are statistical at the 2σ level. Uncertainties on measurements by Eskola et al. were estimated to be 10% to take account of systematic errors (based on this work's approximate 2σ uncertainties using the same CH_3OCH_2Br precursor method).

The lack of significant dependence on pressure at the lowest two temperatures suggests the reaction is at the high pressure limit. Within uncertainties, measurements of k_8 are in agreement with those of Eskola et al.[10] at 295 K. Room temperature measurements in the current work using the CH_3OCH_2Br precursor (solid black triangles in Figure 4) agreed within

uncertainties with those reported by Eskola et al., but were generally (10 – 20)% slower than the method presented here. The lowest pressure k_8 was measured at using CH_3OCH_2Br was significantly lower than the most comparable H_2O_2/H_2O measurement (~35%). The study by Maricq et al.[12] primarily covered higher pressures, but the lowest two pressure measurements are included in Figure 4. The two room temperature measurements made using transient infrared detection of formaldehyde and UV detection of OH, have reasonably large uncertainties, but fall within the range of measurements made in this work (~6–10^{-12} cm^3 $molecule^{-1}$ s^{-1}).

At 450 K, where Eskola et al.[10] made measurements in the fall-off region using He as the bath gas, we also report a positive pressure dependence (442 K data, and 483 K) in N_2. Compared to the literature measurements at 450 K, we measure approximately 5% faster at 442 K, but are in agreement within error at the highest total pressure.

Both this study and previous studies observe a negative temperature dependence for k_8, and positive pressure dependence at higher temperatures over the pressure range tested. The average room temperature $k_8 = (0.94 \pm 0.04) \times 10^{-11}$ cm^3 $molecule^{-1}$ s^{-1}, is in agreement with previous measurements, and significantly faster than other R + O_2 reactions, such as acetyl + O_2 (~$(0.5 – 0.6) \times 10^{-11}$ cm^3 $molecule^{-1}$ s^{-1}) [20,25] and propionyl + O_2 (0.54×10^{-11} cm^3 $molecule^{-1}$ s^{-1}) [20]. Previously, the ionisation potential of the R radical has been correlated with the rate coefficient for R + O_2, where an approximate ionisation potential for CH_3OCH_2 of 7 eV [37,38] would predict ~3×10^{-11} cm^3 $molecule^{-1}$ s^{-1} for k_8 [19]. This estimation is three times higher than k_8 observed here, but is qualitatively in agreement with the DME system exhibiting a much faster rate coefficient than other R + O_2 reactions.

OH yields. OH yields from well-skipping in the DME system were obtained over 4.1 – 32.6 Torr of N_2, and 291 – 483 K (thermal production of OH from stabilised RO_2 radicals begins above approximately 500 K). Treating these data with a Stern–Volmer analysis (Figure 5) demonstrates an increase in yield with increasing temperatures, and the suppression of yields at higher pressures. This is consistent with what would be expected of OH yields from R10, a process deactivated by the pressure–dependent stabilisation of the RO_2* radical (R9). At room temperature (black filled circles, Figure 5), yields were particularly low at higher pressures, which is reflected in the greater uncertainties due to the less pronounced biexponential decays.

Comparison with OH yields obtained by Eskola et al.[10] in nitrogen shows good agreement with the relative measurements conducted using CH_3OCH_2Br photolysis at room temperatures when considering quenching coefficient uncertainties (see Table 2). At ~442 K, the quenching coefficient uncertainty ranges measured in the current work and by Eskola et al. at 450 K are in agreement. Room temperature yields from Maricq et al.[12] were included, and are not close to agreement with this work.

Reciprocal yields were fit using weighted linear analyses, and intercepts are fixed at unity, imposing a 100% OH yield at $[N_2] = 0$ molecule cm^{-3}. The SI includes Stern–Volmer plots with OH yield intercepts floated (S16), where the intercepts were still unity within uncertainties. A comparison of the yields from H_2O_2/H_2O and H_2O_2/urea precursors (S4) is also included.

A pressure range as extensive as that explored by Eskola et al.[10] is not possible using the current method, as the very low yields measured by Eskola et al. (<10%), are difficult to extract from a biexponential decay. This does not affect the quality of the Stern-Volmer plot however, as the lowest pressures obtainable allow [M] to be explored over close to an order of magnitude, and the inset to Figure 5 shows the quenching coefficients extrapolate well to pressures beyond the limitations in this work. At higher temperatures (and therefore yields), this technique will successfully retrieve yields over a wider pressure range.

Comparison with other previous studies of OH yields in the DME system (Table 2) put our measurements close to agreement with data obtained by Rosado-Reyes et al.[14] at room temperature, but not at higher temperatures. The studies by Sehested et al.[11] and Maricq et al.[12] agree poorly with this work's quenching coefficients. The discrepancy with these three studies may be a result of difficult products to detect in their experimental methods, particularly formaldehyde, and the indirect nature of the previous studies.

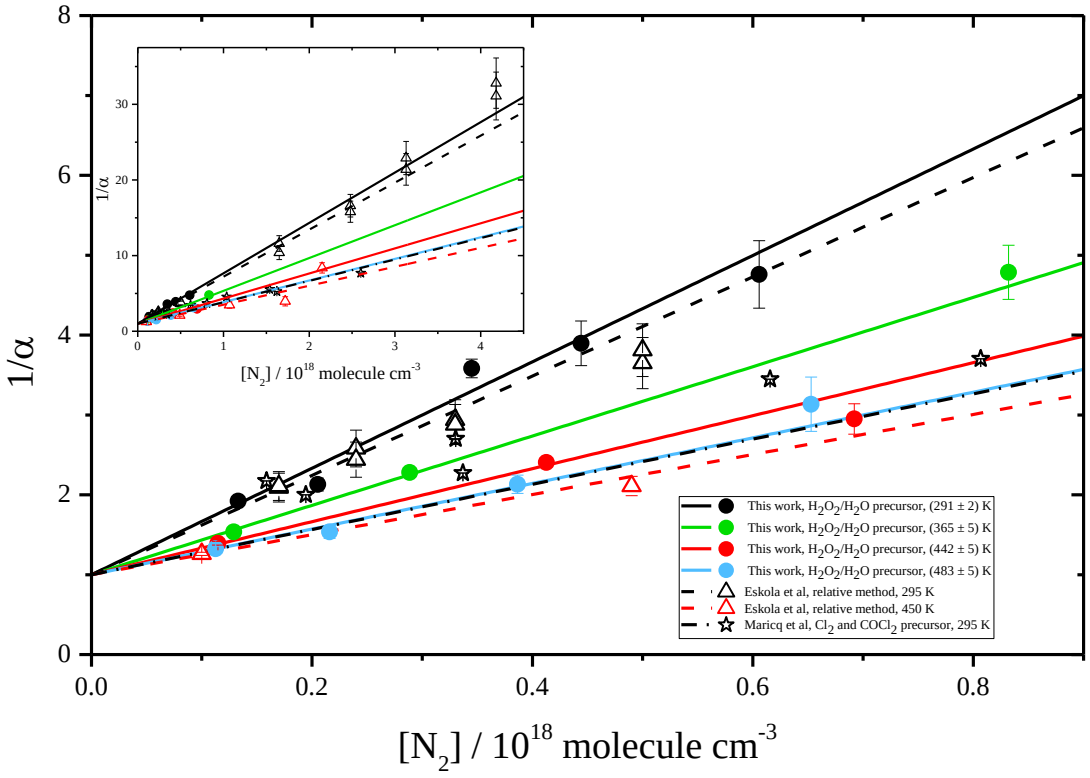

Figure 5. Stern–Volmer plot of OH yields in nitrogen, comparing this work (filled circles, solid lines) to Eskola et al.[10] (open triangles, dashed lines) and Maricq et al.[12] (open stars, dotted line). Inset shows full pressure range of Eskola et al. data. The intercepts are fixed to unity. There are no uncertainties reported for the Maricq et al. data.

The current work does have some limitations, primarily higher pressures cannot be explored using this technique, as a result of the ~10% lower limit on the ability to detect yields (which decrease at higher pressures). Alongside pressure limitations, there is a constraint concerning temperature, where this method will not work above the temperature at which the fuel of interest begins to propagate by a thermal route (R10) via QOOH decomposition. For DME this is approximately 230 °C. To make measurements of well-skipping OH formation above this temperature would require much more complicated analysis, as multiple OH regeneration processes can take place concurrently. If only QOOH decomposition was occurring, then measurements of R + O_2 rate coefficients would still be accurate using the method presented in this work, however yields would be perturbed. If a second oxygen addition (O_2 + QOOH) was taking place, then both yields and rate coefficients would not be accurately measurable using the current analysis method. DME is the simplest ether, but more complex

fuels (such as DEE), would have more than one possible initial abstraction site, and therefore isomers of the R radical. The method presented does not differentiate between different R radical isomers, and as such would present yields and rate coefficients as averaged values.

Table 2. Comparison of quenching coefficients for $CH_3OCH_2 + O_2$ obtained in the current work with previous measurements. M = N_2 for all measurements.

Reference	Precursor	Technique[a]	T / K	P / Torr	k_M/k_C[b]
Sehested et al.[11]	Cl + DME	FTIR	296	0.38 – 940	3.13 ± 0.51
Maricq et al.[12]	Cl + DME	TIR	295	4.9 – 80.3	4.3
			350	5.0 – 50.0	2.9
Rosado-Reyes et al. [14]	Cl + DME	TIR	295	10 – 200	7.15
			450	10 – 200	0.87
Eskola et al.[10]	CH_3OCH_2Br	LIF/RM	295	5.3 – 95.3	6.05 ± 0.54
		LIF/RM	450	unknown	2.51 ± 0.48
	Cl + DME	LIF/AM	295	5 – 25.01	4.71 ± 0.14
		LIF/AM	450	5 – 99.98	2.36 ± 0.12
This work	OH + DME	LIF	291	4.1 – 18.8	6.66 ± 1.06
		LIF	365	4.9 – 31.3	4.34 ± 0.47
		LIF	442	5.3 – 31.5	3.32 ± 0.66
		LIF	483	5.7 – 32.6	2.86 ± 0.35

[a]Abbreviations: FTIR, Fourier transform infrared spectroscopy; TIR, transient infrared; LIF, laser–induced fluorescence; RM, relative method; AM, absolute method. [b]Units are 10^{-18} cm^3 $molecule^{-1}$. Uncertainties are statistical at the 2σ level.

Supporting Information

More details of data and analysis, including further details of Kintecus simulated traces, experimental uncertainty dependence on O_2, room temperature k_8 values, k_x and O_2x from global analysis, comparison of analysis methods and precursors.

Author Information

*(M.A.B) Email address: M.Blitz@leeds.ac.uk

(P.W.S.) Email address: P.W.Seakins@leeds.ac.uk

Acknowledgements

EPSRC Grant No. EP/L014912/1 for funding for D.G.P.

References

[1] S.H. Robertson, P.W. Seakins, M.J. Pilling, in: M.J. Pilling (Ed.), Comprehensive Chemical Kinetics, Elsevier, Amsterdam, 1997.

[2] C.K. Westbrook, Proc. Combust. Inst. 28 (2000) 1563.

[3] J. Zádor, C.A. Taatjes, R.X. Fernandes, Prog. Energy Combust. Sci. 37 (2011) 371.

[4] T.J. He, Z. Wang, X.Q. You, H.Y. Liu, Y.D. Wang, X.Y. Li, X. He, Fuel 212 (2018) 223.

[5] O. Welz, J. Zador, J.D. Savee, M.Y. Ng, G. Meloni, R.X. Fernandes, L. Sheps, B.A. Simmons, T.S. Lee, D.L. Osborn, C.A. Taatjes, Phys. Chem. Chem. Phys. 14 (2012) 3112.

[6] A. Alvarez, A. Bansode, A. Urakawa, A.V. Bavykina, T.A. Wezendonk, M. Makkee, J. Gascon, F. Kapteijn, Chemical Reviews 117 (2017) 9804.

[7] C. Arcoumanis, C. Bae, R. Crookes, E. Kinoshita, Fuel 87 (2008) 1014.

[8] A.J. Eskola, S.A. Carr, M.A. Blitz, M.J. Pilling, P.W. Seakins, Chem. Phys. Lett. 487 (2010) 45.

[9] D.C. Rakopoulos, C.D. Rakopoulos, E.G. Giakoumis, R.G. Papagiannakis, D.C. Kyritsis, Energy 73 (2014) 354.

[10] A.J. Eskola, S.A. Carr, R.J. Shannon, B. Wang, M.A. Blitz, M.J. Pilling, P.W. Seakins, S.H. Robertson, J. Phys. Chem. A 118 (2014) 6773.

[11] J. Sehested, T. Møgelberg, T.J. Wallington, E.W. Kaiser, O.J. Nielsen, J. Phys. Chem. 100 (1996) 17218.

[12] M.M. Maricq, J.J. Szente, J.D. Hybl, J. Phys. Chem. A 101 (1997) 5155.

[13] A. Masaki, S. Tsunashima, N. Washida, J. Phys. Chem. 99 (1995) 13126.

[14] C.M. Rosado-Reyes, J.S. Francisco, J.J. Szente, M.M. Maricq, L. Frøsig Østergaard, J. Phys. Chem. A 109 (2005) 10940.

[15] M.J. Pilling, M.J. Smith, J. Phys. Chem. 89 (1985) 4713.

[16] I.R. Slagle, Á. Bencsura, S.-B. Xing, D. Gutman, Symposium (International) on Combustion 24 (1992) 653.

[17] I.R. Slagle, J.-Y. Park, D. Gutman, Symposium (International) on Combustion 20 (1985) 733.

[18] A.F. Wagner, I.R. Slagle, D. Sarzynski, D. Gutman, J. Phys. Chem. 94 (1990) 1853.

[19] I.R. Slagle, J.R. Bernhardt, D. Gutman, Chem. Phys. Lett. 149 (1988) 180.

[20] M.T.B. Romero, M.A. Blitz, D.E. Heard, M.J. Pilling, B. Price, P.W. Seakins, Chem. Phys. Lett. 408 (2005) 232.

[21] M.A. Blitz, D.E. Heard, M.J. Pilling, Chem. Phys. Lett. 365 (2002) 374.

[22] N.U.M. Howes, J.P.A. Lockhart, M.A. Blitz, S.A. Carr, M.T. Baeza-Romero, D.E. Heard, R.J. Shannon, P.W. Seakins, T. Varga, Phys. Chem. Chem. Phys. 18 (2016) 26423.

[23] J.V. Michael, D.G. Keil, R.B. Klemm, J. Chem. Phys. 83 (1985) 1630.

[24] S.A. Carr, M.T. Baeza-Romero, M.A. Blitz, M.J. Pilling, D.E. Heard, P.W. Seakins, Chem. Phys. Lett. 445 (2007) 108.

[25] S.A. Carr, D.R. Glowacki, C.-H. Liang, M.T. Baeza-Romero, M.A. Blitz, M.J. Pilling, P.W. Seakins, J. Phys. Chem. A 115 (2011) 1069.

[26] G. Kovács, J. Zádor, E. Farkas, R. Nádasdi, I. Szilágyi, S. Dóbé, T. Bérces, F. Márta, G. Lendvay, Phys. Chem. Chem. Phys. 9 (2007) 4142.

[27] M.T.B. Romero, D.R. Glowacki, M.A. Blitz, D.E. Heard, M.J. Pilling, A.R. Rickard, P.W. Seakins, Phys. Chem. Chem. Phys. 9 (2007) 4114.

[28] J. Lockhart, M. Blitz, D. Heard, P. Seakins, R. Shannon, J. Phys. Chem. A 117 (2013) 11027.

[29] J.C. Hansen, Y. Li, C.M. Rosado-Reyes, J.S. Francisco, J.J. Szente, M.M. Maricq, J. Phys. Chem. A 107 (2003) 5306.

[30] D.G. Potter, S. Wiseman, M.A. Blitz, P.W. Seakins, J. Phys. Chem. A 122 (2018) 9701.

[31] S.A. Carr, M.A. Blitz, P.W. Seakins, J. Phys. Chem. A 115 (2011) 3335.

[32] L. Onel, M.A. Blitz, P.W. Seakins, J. Phys. Chem. Lett. 3 (2012) 853.

[33] Z. Hong, A. Farooq, E.A. Barbour, D.F. Davidson, R.K. Hanson, J. Phys. Chem. A 113 (2009) 12919.

[34] W. Ludwig, B. Brandt, G. Friedrichs, F. Temps, J. Phys. Chem. A 110 (2006) 3330.

[35] J.C. Ianni, Kintecus, www.kintecus.com, 2017.

[36] S.A. Carr, T.J. Still, M.A. Blitz, A.J. Eskola, M.J. Pilling, P.W. Seakins, R.J. Shannon, B. Wang, S.H. Robertson, J. Phys. Chem. A 117 (2013) 11142.

[37] D. Griller, F.P. Lossing, J. Am. Chem. Soc 103 (1981) 1586.

[38] F.P. Lossing, J. Am. Chem. Soc 99 (1977) 7526.